ADVANCING EARTH AND SPACE SCIENCES

JGR Solid Earth

RESEARCH ARTICLE

10.1029/2025JB033104

Testing Models for Upper Mantle Earthquakes in the Tanganyika-Rukwa Rift, Africa

Eduardo Arzabala[1], **Cynthia Ebinger**[1], **Finnigan Illsley-Kemp**[2], **Aude Lavayssière**[3], and **Derek Keir**[4,5]

[1]Department of Earth and Environmental Sciences, Tulane University, New Orleans, LA, USA, [2]School of Geography, Environment and Earth Sciences, Victoria University of Wellington, Wellington, New Zealand, [3]Université Côte d'Azur, Observatoire Côte d'Azur, CNRS, IRD, Nice, France, [4]Dipartimento di Scienze della Terra, Università degli Studi di Firenze, Firenze, Italy, [5]School of Ocean and Earth Science, University of Southampton, Southampton, UK

Key Points:

- Active and frozen upper mantle intrusions create differential stresses of 1–10 MPa
- Numerical models match local rotations of mantle fracture orientations
- Upper mantle intrusion zones are weak zones that localize strain

Supporting Information:

Supporting Information may be found in the online version of this article.

Correspondence to:

E. Arzabala,
earzabala@tulane.edu

Citation:

Arzabala, E., Ebinger, C., Illsley-Kemp, F., Lavayssière, A., & Keir, D. (2026). Testing models for upper mantle earthquakes in the Tanganyika-Rukwa rift, Africa. *Journal of Geophysical Research: Solid Earth*, *131*, e2025JB033104. https://doi.org/10.1029/2025JB033104

Received 1 OCT 2025
Accepted 29 MAR 2026

Author Contributions:

Conceptualization: Eduardo Arzabala, Cynthia Ebinger, Derek Keir
Formal analysis: Eduardo Arzabala, Cynthia Ebinger, Finnigan Illsley-Kemp, Aude Lavayssière
Methodology: Eduardo Arzabala, Cynthia Ebinger, Finnigan Illsley-Kemp
Resources: Cynthia Ebinger, Aude Lavayssière
Software: Eduardo Arzabala, Finnigan Illsley-Kemp
Supervision: Derek Keir
Visualization: Eduardo Arzabala
Writing – original draft: Eduardo Arzabala
Writing – review & editing: Cynthia Ebinger, Finnigan Illsley-Kemp, Aude Lavayssière, Derek Keir

Abstract

Rifts that initiate in mechanically strong, stable continental lithosphere are characterized by M > 5 earthquakes at depths >35 km near or below the crust mantle interface. Current models for deep rift zone earthquakes invoke elevated pore pressures associated with magmatism, and rapid stressing from magma intrusions. We evaluate the role of static stress changes caused by lateral density contrasts (magma intrusions) in the upper mantle and crust-mantle interface on mantle earthquakes. We use numerical models of static stress changes, and test models against seismic data from the Tanganyika rift, East Africa which has upper mantle earthquakes and locally elevated crustal Vp/Vs. The earthquake source mechanisms from these ML2.4–2.8 earthquakes show steep nodal planes and little correlation to crustal source mechanisms and E–W extension direction. Likewise, the direction of fast splitting from seismic anisotropy studies is oblique to predictions from earthquake source mechanisms. The models of density contrasts (magma intrusions) explored in this study predict differential stresses of 1–10 MPa, stresses consistent with average earthquake stress drops. The local stress field rotations around the edges of intrusive bodies can explain the variable source mechanisms and match the local rotation of shear wave splitting direction, providing a plausible mechanism for mantle earthquakes in cratonic rifts. By analogy, exhumed mantle from rift zones reveals pseudotachylites near intrusions. Metasomatic reactions in contact aureoles broaden density contrasts and reduce upper mantle strength, potentially enabling extension of initially cold, strong continental lithosphere.

Plain Language Summary

Continental rift zones host rare earthquakes in the upper mantle well below the typical crustal earthquake depths. We investigate a possible mechanism to explain upper mantle earthquakes as the consequence of magma intrusion zones that may accumulate over millions of years. These intrusion zones have densities lower than the surrounding mantle, and they produce pressure gradients that may permanently modify the orientation of stresses in the plate. An earthquake monitoring network captured spatial clusters of upper mantle earthquakes in the Tanganyika-Rukwa rift in East Africa, providing detailed information on earthquake sources and locations with respect to typical crustal earthquakes. Our models of long-lived magmatic intrusion zones, modeled as subsurface density contrasts, are compared to these observations from the Tanganyika-Rukwa rift. Our results suggest that the stress concentrations around the edges of magma bodies can explain both the earthquake locations as well as the observed rotations in the orientations of mantle fractures.

1. Introduction

Continental rifting in parts of East Africa initiates in thick, strong lithosphere whose combined strength is more than plate driving forces, a long-standing tectonic conundrum (e.g., Bialas et al., 2010; Bott, 1990). Earthquakes in the lower crust and upper mantle of early-stage rift zones developing in strong lithosphere provide new insights. The depth distribution of earthquakes in continental lithosphere provides constraints on the depth to the brittle-ductile transition zone and plate rheology (e.g., Albaric et al., 2010; Bürgmann & Dresen, 2008). The rheology of Earth's crust and upper mantle is controlled by the rock composition, thermal structure, fluid content, and strain rate (e.g., Bürgmann & Dresen, 2008). Despite elevated lithospheric geotherms that reduce plate strength in continental rift zones, earthquakes at depths of 30–60 km have been documented with global networks (Craig & Jackson, 2021; Wang & Klemperer, 2026; Yang & Chen, 2010) and local arrays in several sectors of the Baikal rift, East African rift, and beneath the flanks of the Red Sea rift (e.g., Blanchette et al., 2018; Déverchère

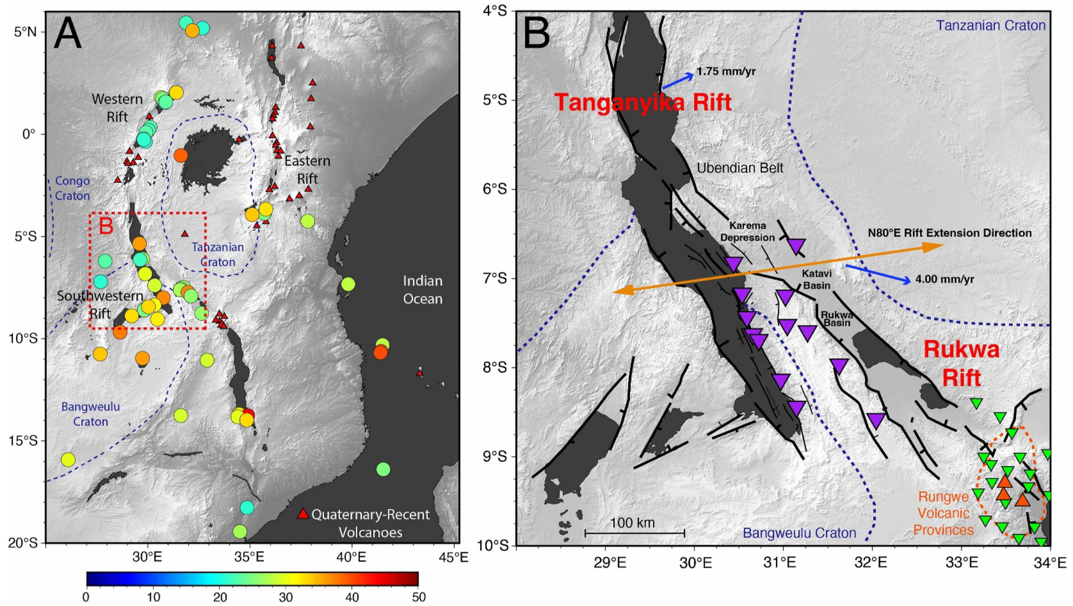

Figure 1. (a) Distribution of teleseismically detected earthquakes at depth ≥20 km in the East African rift system with respect to Archean cratons and Quaternary-Holocene eruptive centers (red triangles). Lower crustal and upper mantle (depth >20 km) earthquakes since 1964 determined from waveform modeling are color-coded by depth from the compilation of teleseisms from Yang and Chen (2010) and Craig and Jackson (2021). (b) Border faults and major intrabasinal faults of the Tanganyika-Rukwa rift with respect to Archean cratons and Proterozoic Ubendian orogenic belt, and Rungwe volcanic province (orange triangles) (after Lavayssière et al., 2019). TANGA14 seismic array is denoted as inverted purple triangles; a subset of SEGMeNT seismic stations (Shillington et al., 2016) is plotted as inverted green triangles. Extensional GNSS velocity vectors from a Nubia-fixed reference frame are shown in blue based on campaign GNSS measurements (Stamps et al., 2018). Kostrov summation of earthquakes (local and teleseismic) indicate an approximately N80°E rift extension direction shown in orange (Lavayssière et al., 2019).

et al., 1991; Lavayssière et al., 2019) (Figure 1a). However, the lack of data on crustal thickness in many areas leaves questions remaining regarding which side of the crust-mantle boundary deep-rift earthquakes occur, with fundamental implications for lithospheric rheology.

Lower crust and upper mantle seismicity has been linked to the presence of pressurized magma bodies (e.g., Weinstein et al., 2017), ductile strain localization due to heating (e.g., Hutchings et al., 2025), the percolation of magmatic fluids (e.g., Lindenfeld et al., 2012), or the presence of lateral density heterogeneities that lead to strain localization (e.g., Buck, 2004; Oliva et al., 2022). We can further understand processes associated with earthquakes at the crust-mantle boundary and within the upper mantle using earthquake source mechanisms and shear wave splitting directions that coincide with the orientations of fluid-filled fractures that form in the local stress field around intrusions (e.g., Illsley-Kemp et al., 2019).

Teleseismically-detected rift zone earthquakes at depths greater than 20 km may have location errors of 10–35 km in many regions, and these uncertainties prevent determination of locations relative to the base of the crust beneath the extensional basins or the largely unthinned crust beneath the uplifted rift flanks (e.g., Craig & Jackson, 2021; Yang & Chen, 2010). Local seismic arrays provide the location accuracy needed, but they are generally temporary arrays and so provide only a snapshot of a much longer process.

The southern Tanganyika-Rukwa rift, part of the Western rift is one of the most seismically active regions in the East African rift system with 13 earthquakes since 1910 of $4.8 < M_w < 6.8$ at well constrained depths of 8–37 km determined from waveform modeling of teleseismic arrivals (Craig & Jackson, 2021; Yang & Chen, 2010) (Figure 1). Seismicity data from a temporary array reveal a seismogenic zone spanning the surface to 57 km depth, with a clear gap between the lower crustal seismicity at 27–40 km depth, and the upper mantle seismicity at 47–57 km depth (Lavayssière et al., 2019). Seismicity, therefore, spans the entire crustal thickness, with the most energetic earthquakes near the crust-mantle boundary along projections of the border fault to the base of the crust (Lavayssière et al., 2019). This region experienced a M_w 7.4 earthquake in 1910 that led to widespread ground

10.1029/2025JB033104

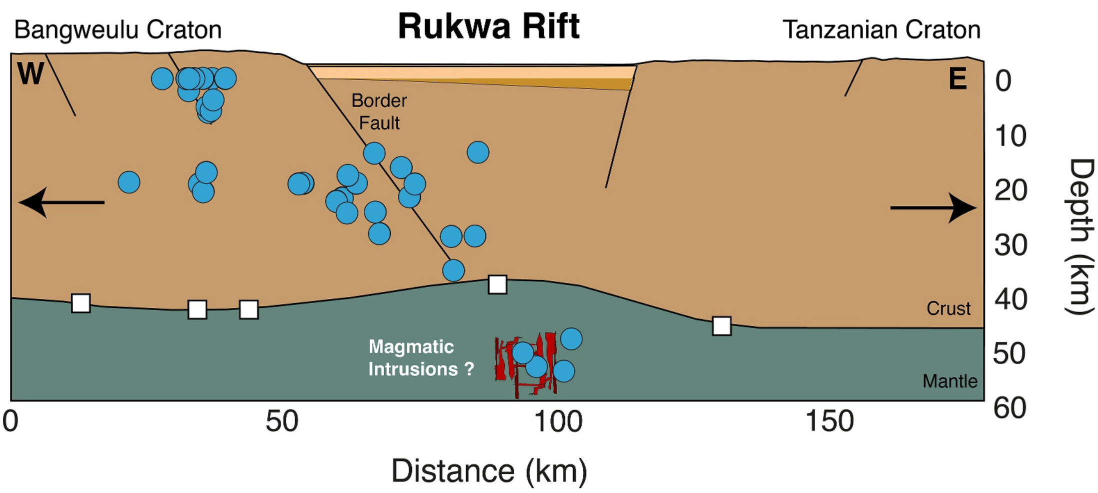

Figure 2. Schematic cross-section through the northern Rukwa basin showing inferred magmatic intrusions (not drawn to scale) comprised of both frozen and hot magmatic intrusions along with upper and lower crustal earthquakes (blue circles) (after Lavayssière et al., 2019). Black arrows represent extensional forces. Squares indicate estimates of Moho depth from receiver function data (Hodgson et al., 2017).

shaking and a submarine landslide that caused a telecommunications cable break along the Indian Ocean coast 800 km to the east (Ambraseys, 1991); a better understanding of mantle earthquakes and their relation to rift border faults is important for earthquake hazard assessment.

Although migrating swarms of earthquakes lacking a mainshock-aftershock sequence are interpreted as active magma intrusions (e.g., Belachew et al., 2011), few studies have considered the link between lower crust and upper mantle earthquakes and the presence of static density contrasts created by long-lived magmatic sill and dike complexes. During and after intrusion Coulomb failure stress changes may trigger slip along favorably oriented faults (e.g., Woods et al., 2019), but our focus is on the long-term implications of cooling or frozen sill and dike complexes on state-of-stress. That is, we simulate the consequences of multiple magma intrusions into the mantle lithosphere on longer term stresses. Studies of crustal intrusion zones show that lateral pressure gradients around the margins of hot (low density) and frozen (high density) magma intrusions may cause stress concentrations that localize strain, as marked by enhanced seismicity (e.g., Beutel et al., 2010; Oliva et al., 2022). Evidence from crust and upper mantle from an ancient rift now exhumed in Norway hosts pseudo-tachylites along the edges of dikes in the uppermost mantle, offering insights into what may be occurring beneath the Western rift (Sørensen et al., 2019). We develop numerical models to predict the state of stress around magma intrusion zones simulated by a range of mantle density contrasts with dimensions and properties of sill and dike complexes imaged in other rifts and then compare the models to earthquake source mechanisms and shear wave splitting patterns of earthquakes in the lower crust and upper mantle beneath the Tanganyika-Rukwa rift zone. Our work provides new insights into the processes enabling extension in cold, thick cratonic lithosphere, and to the role of mantle heterogeneities, such as deep magmatic sill and dike complexes or pre-existing density contrasts, on strain localization in rift zones.

2. Geodynamics and Tectonic Setting

The low seismic velocity zone rising from the lower mantle beneath southern Africa to the base of the lithosphere in central and northeast Africa is interpreted as a mantle plume that has led to magmatism and extension within the East African rift system (e.g., Boyce et al., 2023; Chang et al., 2020). The seismically and volcanically active East African rift comprises both onshore and offshore sectors, with lower crust and upper mantle earthquakes occurring in sectors on or near Archean cratons (e.g., Lavayssière et al., 2019; Wang & Klemperer, 2026; Yang & Chen, 2010) (Figure 1a).

The Western rift system developed within ~120–140 km-thick Proterozoic orogenic belts between the 160–200 km-thick Archean Tanzanian, Congo, and Bangweulu cratons, based on seismic data calibrated with xenolith data (Afonso et al., 2022) (Figures 1 and 2). At the surface, the Proterozoic crust displays strain fabrics spanning NNW to NW in the Ubendian belt, and an east-west orientation along the southern boundary of the

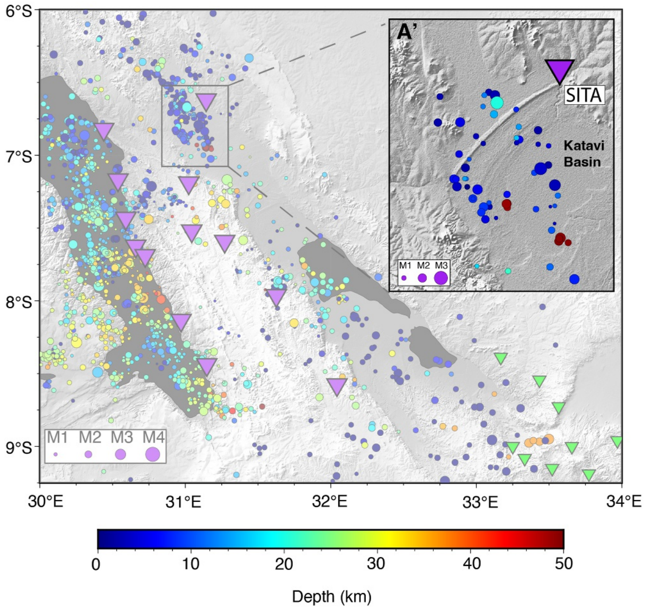

Figure 3. Absolute locations of TANGA14 earthquake catalog of Lavayssière et al. (2019) with size scaled relative to local magnitude and colored by depth. Location uncertainties are <2 km. TANGA14 array that operated from June 2014–September 2015 are shown by purple inverted triangles; smaller inverted green triangles denote SEGMeNT stations used in locations. (A′) inset displays precise earthquake relocations from double difference analyses for the Katavi basin region scaled by magnitude and color coded by depth after Lavayssière et al. (2019). Upper mantle earthquakes are colored red.

Tanzania craton (e.g., Boniface et al., 2014). Parts of the rift transect Permo-Triassic rift basins, like the Rukwa rift that contains up to 10 km of Mesozoic and Cenozoic sedimentary strata (Mtelela et al., 2016).

The only surface expression of magmatism in this rift sector are ∼25 My carbonatitic tuffs in the southern Rukwa area that mark the onset of rifting (Roberts et al., 2010). In the Tanganyika rift, constraints on the initiation of faulting and basin formation by ∼16 Ma come from the extrapolation of <1.6 Ma depositional rates to the base of 5–7 km thick sedimentary basins (Scholz & Lyons, 2010). Despite the isolated volcanic occurrences, multiple lines of evidence suggest that the lithosphere beneath the Tanganyika-Rukwa-Malawi region has been modified by CO_2-rich fluids from the mantle plume. The Rukwa rift is the site of a M_b 4.7 mantle earthquake (15 October 2021) analyzed using the ratio of the Sn and Lg seismic wave amplitudes on global networks (Wang & Klemperer, 2026). They measure small Sn excitations likely due to attenuation by partial melt in the upper mantle or scattering in the crust (Wang & Klemperer, 2026). Geochemical analyses of hot springs and volcanic rocks indicate metasomatism from the percolation of CO_2-rich fluids (Furman, 1995; Innocenzi et al., 2024).

The South Tanganyika rift comprises half-graben basins delineated by large offset normal fault systems (e.g., Morley, 1988; Muirhead et al., 2019). The Rukwa rift is bounded on its eastern side by a NW-striking Mesozoic fault, and on its western side by a seismically active NNW-striking border fault (e.g., Delvaux et al., 2012; Lavayssière et al., 2019) (Figures 2 and 3). It is linked by dextral oblique-slip faults to the Tanganyika rift through the Karema depression (Delvaux et al., 2012) (Figure 1b). Stress inversion and Kostrov summation of source mechanisms of 29 local crustal earthquakes that occurred between 2013–2014 and 2024 teleseismically-detected earthquakes that occurred between 1973 and 2018 indicate a regional extension direction oriented ∼ N80° (Lavayssière et al., 2019) closely aligned with the sub E–W opening direction of ≤4 mm y^{-1} derived from campaign and continuous geodetic data (Stamps et al., 2018) (Figure 1b).

Mantle anisotropy patterns determined from SKS-splitting measurements are consistent with asthenospheric flow around cratonic roots, with delay times possibly enhanced by oriented melt pockets beneath the Rungwe Volcanic Province (Tepp et al., 2018) (Figure 1). Ajala et al. (2024) argue that the elevated flanks of the southern Tanganyika rift and negative free-air gravity anomalies can be explained by the presence of a local upper mantle thermal anomaly and its isostatic effects, whereas Ebinger et al. (1991) explain the topography and free air anomalies as flexural uplift of stretched, strong lithosphere superposed on a much broad dynamic upwelling.

Constraints on crustal thickness are lacking beneath the Tanganyika and Rukwa lake basins, but receiver function results onshore indicate that the crust thins from approximately 41 km on the rift flanks to 27 km beneath the fault-bounded southern Tanganyika basins, representing an extension of about 32% (Hodgson et al., 2017). Crust beneath several areas within and near the Rukwa and Tanganyika rifts have higher V_P/V_S ratios ranging from 1.84 to 1.97, suggesting a mafic and ultramafic lower crustal composition that may indicate Miocene-Recent mafic intrusions (Hodgson et al., 2017). Crustal shear-wave splitting analyses of local earthquakes revealed fast polarization parallel to NNW-striking rift structures and with largest delay times for lower crustal earthquakes in areas with higher V_P/V_S, after normalization for the entire ray path, suggesting fluid-filled cracks may contribute to the measured anisotropy (Ajala et al., 2024).

Further suggestions of crust and mantle magmatism come from seismicity distributions. Seismicity data reveal a concentration of seismic activity in the lower crust and mantle lithosphere beneath southern Lake Tanganyika, as well as a distinct mantle earthquake cluster at the northern end of the Rukwa rift beneath the Katavi basin (Lavayssière et al., 2019) (Figure 1b). The border faults, which have accommodated most of the extension (Ebinger et al., 1991; Morley, 1988; Muirhead et al., 2019), are associated with steep nodal planes (≥45°) to depths of 35 km (Lavayssière et al., 2019). Our new analyses focus on the deepest cluster of earthquakes at depths 47–57 km that are clearly within the mantle, supplementing earlier work by Lavayssière et al. (2019) (Figure 2).

3. Magmatic Intrusions: A General Overview

In areas of continental extension, magma transport from the asthenosphere and mantle lithosphere to the surface through diking plays a key role in facilitating extension in continental rifts (e.g., Bialas et al., 2010; Rivalta et al., 2015). Field mapping and geophysical imaging of crustal intrusions provide constraints on the geometry and kinematics of dike intrusion (e.g., Magee et al., 2013; Qin et al., 2020; Valentine & Krogh, 2006). Magma intrusion into the mantle and lower crust, however, produces surface deformation signals at or below the detection threshold of InSAR and most continental crustal imaging (e.g., Ebmeier et al., 2018). Analyses of lower crustal and upper mantle rocks from an ancient magmatic rift exhumed in Scandinavia and seismically imaged frozen magmatic intrusions provide important clues about these deep rift zone processes (e.g., Gase et al., 2019; Menegon et al., 2021; Sørensen et al., 2019).

In the simplest sense, magmatic intrusions are hot, compressible fluid with exsolving gases that intrude relatively colder rocks that behave elastically in response to rapidly applied stresses (Rivalta et al., 2015). The orientation of active and cooling or frozen (static) magma bodies is largely influenced by the subsurface state of stress; magmatic intrusions propagate perpendicular to the direction of the minimum principal stress (e.g., Rubin, 1995; Valentine & Krogh, 2006). Not only are magmatic intrusions influenced by the state-of-stress, but they can rotate the local stress field and alter the intrusion's propagation direction (e.g., Magee et al., 2013; Oliva et al., 2022). The magma's high temperature also affects the adjacent host rock through contact metamorphism degassing and vein formation, leading to a local reduction in strength (e.g., Sørensen et al., 2019; Whitney et al., 2003). Rift extension, volatile exsolution, and heating may lead to the formation of fluid-filled cracks that create a mechanical anisotropy whose presence can be detected by shear-wave splitting (e.g., Kendall et al., 2006).

In three dimensions, the thicknesses of dikes and sills are much less than their height and length (Rivalta et al., 2015). Geophysical observations show that an intrusion's thickness or opening (from a bird's-eye point of view) typically ranges from centimeters to meters or even tens of meters; their length or vertical propagation ranges from hundreds of meters to kilometers, and their height is generally of the same magnitude as their length (e.g., Belachew et al., 2011; Brown & Kim, 2020; Toda et al., 2002; Wrona et al., 2019). Magmatic intrusions are rarely isolated and, instead, are part of a bigger magmatic complex comprising stacked sills linked by dikes (e.g., Jolly & Sanderson, 1995). We use these outcrops and imaged data sets as well as knowledge of the state-of-stress around intrusions of higher or lower density to constrain our 2D static models of both vertical planes that simulate a single dike (modeling for length and height) or sill-shaped complexes made of hot and solidified interconnected dikes and sills that formed as a result of tectonic and magmatic interactions (Figure 2).

4. Data

We use the earthquake catalog comprising 2,213 earthquakes from the June 2014 to September 2015 TANGA14 seismic experiment (Figure 3). For the TANGA14 experiment, broadband Guralp CMG 3ESP and 6T, seismometers recorded data at a sample rate of 50.0 Hz and for the SEGMeNT experiment, Guralp 3T, STS-2, and Trillium 40 seismometers recorded at 100 Hz (e.g., Ebinger, 2014; Gaherty et al., 2013). Stations from the SEGMeNT array were also used for earthquake locations and source mechanisms. The seismic stations within each array were spaced ∼30–50 km apart with the combined arrays covering most of the remote area between Lake Tanganyika and Lake Rukwa (Figure 3). The earthquake catalog, including a new velocity model, magnitude scaling and precise relocations determined using waveform cross-correlation and double-differencing are described in Lavayssière et al. (2019). We rely on double difference relocations that have mean relative error of 115 m N–S, 160 m E–W, and 220 m in depth for events in the crust, and 120 m N–S, 195 m E–W and 215 m in depth in the upper mantle, assuming a uniform uppermost mantle velocity structure (Lavayssière et al., 2019).

5. Methods

5.1. Source Mechanisms

Source mechanism solutions from upper and lower crustal earthquakes are found in Lavayssière et al. (2019). For the earthquakes in the upper mantle, none of the events generated surface waves adequate for waveform modeling to evaluate contributions from non-double-couple components. We instead use the first-motion modeling program FOCMEC (Snoke, 1984), which assumes a double-couple solution. The take-off angle and back azimuth from the NonLinLoc location and polarity of the vertical component waveforms are used in the grid search

Table 1
Material Parameters

Layers	Density (kg/m3)	Vs (km/s)	Vp (km/s)	References
Crust	2,800	3.5	6.3	Brocher, 2005; Hodgson et al., 2017
Mantle	3,300	4.5	8.1	Brocher, 2005; Hodgson et al., 2017
Hot Intrusion	2,661	3.6	6.2	Brocher, 2005; Roecker et al., 2017
Med-Hot Intrusion	2,980	4	7.15	Brocher, 2005; Roecker et al., 2017
Cool intrusion	3,139	4.2	7.6	Brocher, 2005; Roecker et al., 2017

algorithm to solve for the best-fitting nodal planes, and P and T axes. Earthquakes with clear P-arrivals on 8 or more stations and with azimuthal gaps ≤120° were screened for focal mechanism solutions. Four of the upper mantle earthquakes had strike, dip, and rake of the better-constrained slip plane with $2\sigma \leq 20°$ (Table 2).

5.2. Seismic Anisotropy

Seismic anisotropy is the directional dependence of seismic wave speed and is often measured using the detection of shear-wave splitting (e.g., Illsley-Kemp et al., 2017, 2019). There are multiple physical mechanisms which can cause seismic anisotropy, including aligned structural features (Boness & Zoback, 2006), and fluid-filled microcracks (Crampin & Peacock, 2008; Dunn et al., 2005). In this study we measure the seismic anisotropy recorded by the shear-wave splitting of local earthquakes near station SITA, the closest station to the upper mantle earthquakes (Figure 3). In particular, we investigate whether there is any variation in the direction or delay time of the seismic anisotropy with depth.

We used the Multiple Filter Automatic Splitting Technique on 132 events (Savage et al., 2010). MFAST develops upon the method of (Teanby et al., 2004) to perform an automatic measure of shear-wave splitting, as well as an assessment of measurement quality. MFAST trials a set of 14 filters and determines the three highest-performing filters based on signal-to-noise ratio. These three filters are then used to measure shear-wave splitting by applying the Silver and Chan (1991) measurement method over multiple time-windows. Finally, a rigorous cluster analysis is performed to grade measurements. The grading identifies measurements that produce significantly different shear-wave splitting results from small changes in other parameters. Our final analysis is limited to measurements of the highest quality (labeled as A), and those with an incidence angle of less than 20° that best sample the crust beneath station SITA. This means that we can be confident that our shear-wave splitting measurements are not the result of specific parameter choices and that they are sampling the subsurface beneath SITA.

5.3. Modeling

5.3.1. Numerical Model Assumptions and Limitations

The objective of our numerical modeling is to evaluate the hypothesis that lateral density contrasts of active and frozen magma bodies in the mantle and lower crust contribute to the deep earthquakes observed in the strong lithosphere beneath the Tanganyika-Rukwa rift. Specifically, we consider the dimensions and magnitude of geologically constrained density contrasts required to induce stress differentials of order 1–10 MPa. This range was selected to reflect the average range of earthquake stress drops for small-magnitude events (e.g., Abercrombie et al., 2025; Baltay et al., 2024). In this work, we approach earthquake stress drops as the change in average stress resolved onto the fault before and after an earthquake (i.e., static stress drops) (Baltay et al., 2024).

We use static numerical models, as our goal is not to model magma propagation in time and space, but rather to evaluate the plausibility that stress concentrations along the margins of hot to frozen magma intrusions are the cause of upper mantle and lower crustal earthquakes. To understand stress concentrations induced by lateral density contrasts we rely on contemporary constraints for model geometry and physical properties (e.g., H-κ analysis, xenolith studies, source mechanisms, seismic anisotropy). Leveraging elastic models allows us to analyze and quantify the effect of density contrasts as an individual component of the stress field, and to linearly superimpose other stress-inducing mechanisms like extensional forces and crustal thinning (e.g., Oliva et al., 2022). The numerical models employed in our study do not capture the dynamic aspects of dike propagation associated with rapid stressing and heating; faults or Coulomb failure stress changes are not incorporated into the

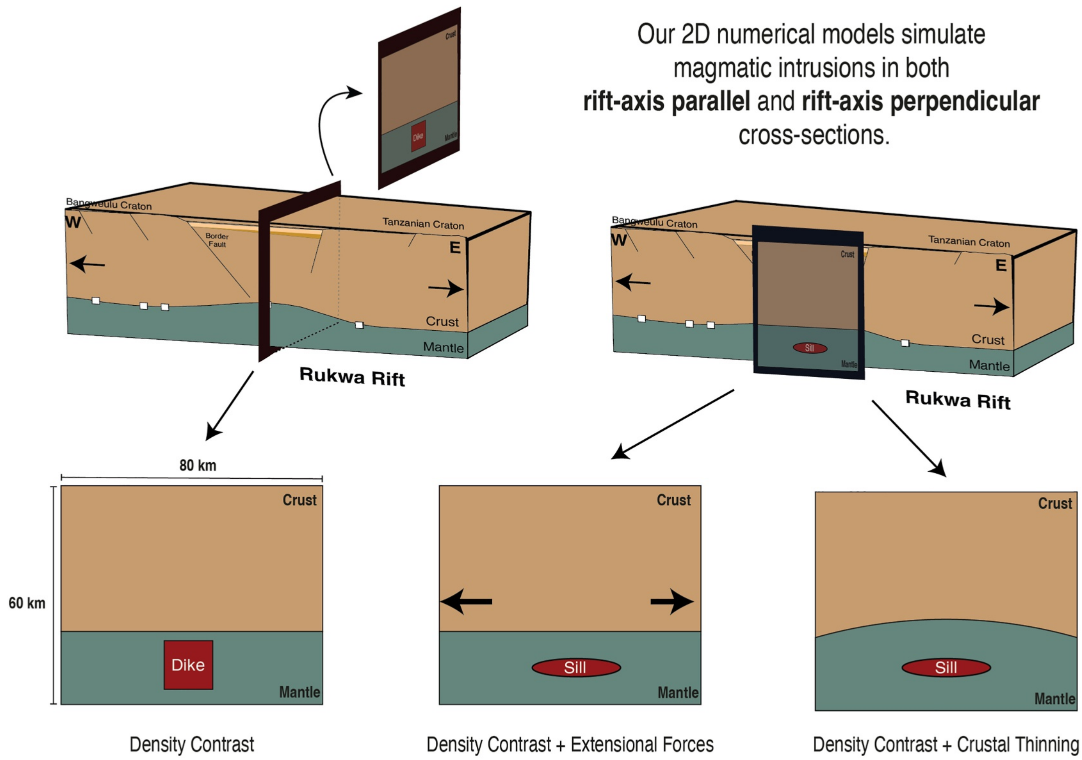

Figure 4. PyLith model approach. Areas of density contrast (red) were placed at depths of lower crustal and upper mantle earthquakes in the Tanganyika-Rukwa study area (only showing a density contrast in the upper mantle). Magmatic intrusions were varied in terms of bulk density, size, geometry, orientation, and depth emplacement.

numerical model. Instead, our focus is the differential stresses emerging from regions of density contrasts and their contribution to over all state-of-stress. Topographic loads are not considered in this study because our depth of interest is 30–60 km, well beyond the depth where topographic loads affect the state of stress in extended continental lithosphere (Oliva et al., 2022). These static models should be considered as first order approximations that explore depth and lateral extent of density contrasts rather than volume. Furthermore, our models do not account for a magma source, which remains unconstrained in the study area (e.g., Rivalta et al., 2015).

A subsurface density heterogeneity generates a body force due to its density contrast with the surrounding rock, and the total horizontal force that it generates can be quantified, analytically, by the area under the stress versus depth profile (Fialko & Rubin, 1999; Turcotte & Schubert, 2002) (Figure SM1 in Supporting Information S1). Taking the example of a two-layer model, where each layer has a uniform bulk density, we can calculate the horizontal force generated by an intrusion by subtracting the integrated pressure of the column with a magmatic intrusion to the integrated pressure of a reference column (Figure SM1 in Supporting Information S1). The resulting difference (ΔF) is the differential force per unit length associated with the intrusion. An analytical calculation is shown in (Figure SM1 in Supporting Information S1).

5.3.2. Numerical Model

The 2D numerical model was developed using PyLith 4.2.0, which is an open source, finite element code for dynamic and quasistatic simulations of lithospheric deformation published under the MIT license (Aagaard et al., 2024). Our modeling goals were to estimate stress differentials that arise from upper mantle and lower crustal magmatic intrusions and compare with (a) deep earthquake locations; (b) state of stress; and (c) variations in crustal anisotropy, assuming it is a measure of fluid-filled fracture orientation. Magmatic intrusions are modeled as areas of density contrasts that can be interpreted to be a dike or sill complex and their contact metamorphic aureoles (Figure 4). The dimensions are constrained by observations of the upper mantle of ancient rift zones exposed by orogenesis and from dimensions of lower crustal and upper mantle sill complexes (e.g., Brown & Kim, 2020; Gase et al., 2019; Magee et al., 2016; Qin et al., 2020; Wrona et al., 2019).

Table 2
Upper Mantle Earthquake Solutions and Classification

ID	Date	hh:mm	lon (°)	lat (°)	depth (km)	Fault/Auxiliary Plane strike	dip	rake	ML	loc	#Sol	#P
M01	06 August 2014	13:28	31.0469	−6.877	53	315	53	−16	2.8	DD	30	13
						54	77	−142				
M02	26 May 2015	6:44	31.0486	−6.877	53	242	41	−12	2.5	DD	16	12
						341	82	−130				
M03	03 June 2015	7:40	31.1558	−6.95208	53	81	81	70	2.8	DD	20	13
						328	22	155				
M04	06 June 2015	3:30	31.1433	−6.957	52	340	18	33	2.4	DD	1	12
						218	80	105				

ID	P axis	T axis	Faulting-type Classifications (Zoback, 1992)
M01	282/36	180/16	Strike-slip: E–W Shortening, N–S Stretching
M02	215/39	102/26	Strike-slip toward transtension: E–W Stretching, N–S Shortening
M03	188/33	329/50	Reverse Faulting: N–W Shortening
M04	295/34	146/52	Reverse Faulting: ESE–WNW Shortening

In addition to varying the dimensions of our density contrasts, we also vary their shape (e.g., rectangular or saucer-shape) and their depth emplacement and consider the individual and combined effects of lateral density heterogeneities, extensional forces, and crustal thinning on the overall state-of-stress (Figure 4). Our 2D modeling approach is appropriate since dike intrusions are sheet-like intrusions in the subsurface. Moreover, our approach allows us to model differential stresses at the edges of lateral density heterogeneities without having to constrain the volume of magma intrusion underneath the Tanganyika-Rukwa rift which is currently unknown.

5.3.3. Numerical Model Components

The static 2D models are 80 km in cross-sectional length and 60 km deep; these dimensions were chosen to avoid model edge effects (Aagaard et al., 2024). For all models, Dirichlet boundary conditions were imposed on the bottom and both sides of the domain, and a free surface was imposed on the top. For models without extension, the lateral boundaries had a zero-displacement boundary condition, and extensional models had four m of displacement imposed on each lateral side which corresponds to a ∼3 MPa horizontal lithospheric stress (e.g., Oliva et al., 2022). PyLith static model parameters include layer thicknesses, bulk densities, and seismic velocities. The models are made of two layers comprising crust and mantle. For models with crustal thinning, Moho depth is taken from H-k analysis from Hodgson et al. (2017) and the crust thins symmetrically from both flanks toward the center, where it reaches a minimum thickness of 35 km. Crust and mantle bulk density (ρ) were estimated from seismic velocities in the Tanganyika rift (Hodgson et al., 2017) and using the empirical velocity-density relations of Brocher (2005). The 2D numerical model meshes are created with triangular elements using GMSH, an open-source finite element mesh generator with a built-in CAD engine and post-processor (Geuzaine & Remacle, 2009). The discretization size is set to 500 m to keep the model computationally efficient.

For our static models, we take the approach of varying the density of the rectangular area from a hot state to a cool state (e.g., Beutel et al., 2010) to get a sense of the evolution of stress around an intrusion over time through a static modeling approach. The magmatic complex geometry and depth of emplacement were also varied to determine depth-dependent minimum dimensions that can result in stress concentrations comparable to typical earthquake stress drops of 1–10 MPa (Figure 4). Magmatic intrusion values were adapted from sill dimensions and velocities determined from seismic studies in the magmatic Natron-Manyara rift on the eastern side of the Tanzania craton (Roecker et al., 2017). Material parameters are given in Table 1.

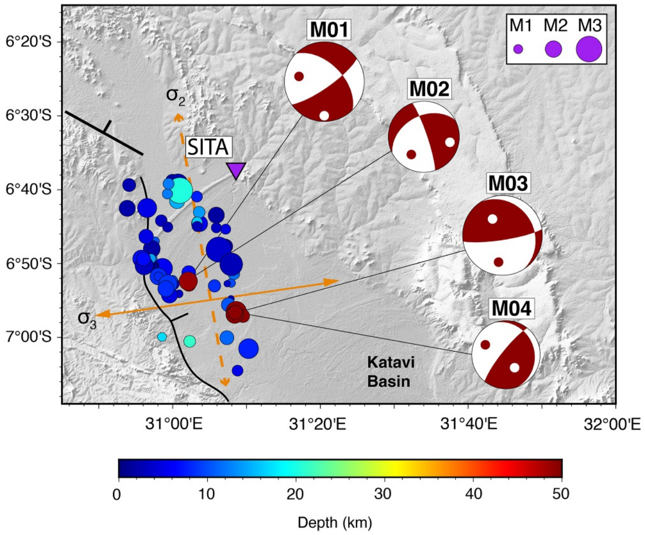

Figure 5. Source mechanisms of upper mantle earthquakes located using double-difference methods in the Katavi basin with P-compression (red dot) and T-dilatation (white dot) axes (M01, M02, M03, M04). The orange line, orientation of σ_3, comes from stress inversion results of teleseisms from 1977 to 2017 that span 8–37 km after Lavayssière et al. (2019). The orange lines, along σ_2 and σ_3, show the vertical cross section used to plot the earthquake source mechanisms to depth on Figure 8.

5.3.4. Post-Processing

Stress concentrations here are defined as the differential stress that arises due to an area of different density. In 2D, PyLith outputs the Cauchy stress components σ_{xx}, σ_{yy}, and σ_{xy} (Aagaard et al., 2024). Principal stress orientations in two dimensions ($\sigma_{1,\ \text{maximum stress}}$, and $\sigma_{2,\ \text{minimum stress}}$) are calculated from PyLith's output Cauchy stress values by composing the 2D stress tensor and computing the respective eigenvectors and eigenvalues at every node in our mesh. To avoid any confusion and adhere to common notation, our σ_2 will be referred to as σ_3 since σ_3 is known as the least compressive stress. The greatest compressive stress, σ_1, is taken to be the preferred orientation of magmatic intrusions which is perpendicular to the preferred opening direction and the orientation of the least compressive stress, σ_3.

6. Results

6.1. Source Mechanisms

All events analyzed occurred within the Rukwa Basin and clustered spatially into two distinct groups, but they are widely separated in time unlike the swarms typical of active magma intrusions (Table 2). The first event, a magnitude 2.8 M_L earthquake occurred on 6 August 2014 (Event M01, Figure 5). Three events occurred in 2015: the magnitude 2.5 M_L earthquake on 26 May (Event M02, Figure 5), the magnitude 2.8 M_L earthquake on 3 June (Event M03, Figure 5), and the magnitude 2.4 M_L earthquake on 6 June (Event M04, Figure 5).

The source mechanism solutions for upper mantle earthquakes exhibit nodal planes with both sub-vertical and ≤20 dips, with strike varying from 80° to 340°. They show significant obliquity to the ∼N80° extension direction within the Tanganyika-Rukwa rift and differ from the crustal earthquake source mechanisms of NNW–SSE to N–S normal and strike-slip orientations (Lavayssière et al., 2019).

6.2. Seismic Anisotropy

In the Tanganyika-Rukwa rift we measured 22 high-quality seismic anisotropy measurements beneath station SITA (Figure 6a). We plot the fast shear-wave orientation (φ) and delay times (δt) as a function of depth to better understand orientations of stress-aligned, fluid-filled microcracks in the uppermost mantle (Figures 6c and 6d). The shear-wave splitting delay time, expressed in seconds, serves as a measure of the magnitude of seismic anisotropy. For each measurement we calculate the standard error of the mean and plot this as an upper and lower error bar (Figures 6c and 6d).

The fast orientation, φ, varies with depth. In the upper 20 km of the crust, φ ranges between -N40° and N70° representing an hour-glass pattern centered on about N15, which is roughly perpendicular to the modern extension direction. Note that NW-striking faults on the eastern side of Rukwa rift formed in Mesozoic times but are largely inactive; the Miocene-Recent faults are sub-N–S (Figure 1b). This agrees with the previous anisotropy study of Ajala et al. (2024) using the same data set. For the four events in the lower crust, the fast direction is between −60° and 60°, with all but one event between 0 and 60°E. The eight events in the upper mantle have φ between 0° and 40° (Figure 6b). Furthermore, we observe no depth-dependent trend in the delay times (δt) across the measured shear-wave splitting events (Figure 6c). The number of observations in these depth divisions is small, however, and the variations may not be significant. Given the similarity of crust and uppermost mantle splitting results, we do not explore models of two-layer splitting.

6.3. Numerical Model Results

All simple geometric models produce similar stress concentration patterns with the largest magnitude stress concentration along the vertical edge of the intrusion represented by a density contrast, with larger magnitudes on the shallowest edges (Figure 7). The stress concentrations induced by a complex or dike of dimensions 8 km by 6 km, 4 km by 8 km, and 2 km by 8 km placed in the lower crust, crust-mantle boundary, or upper mantle are all of

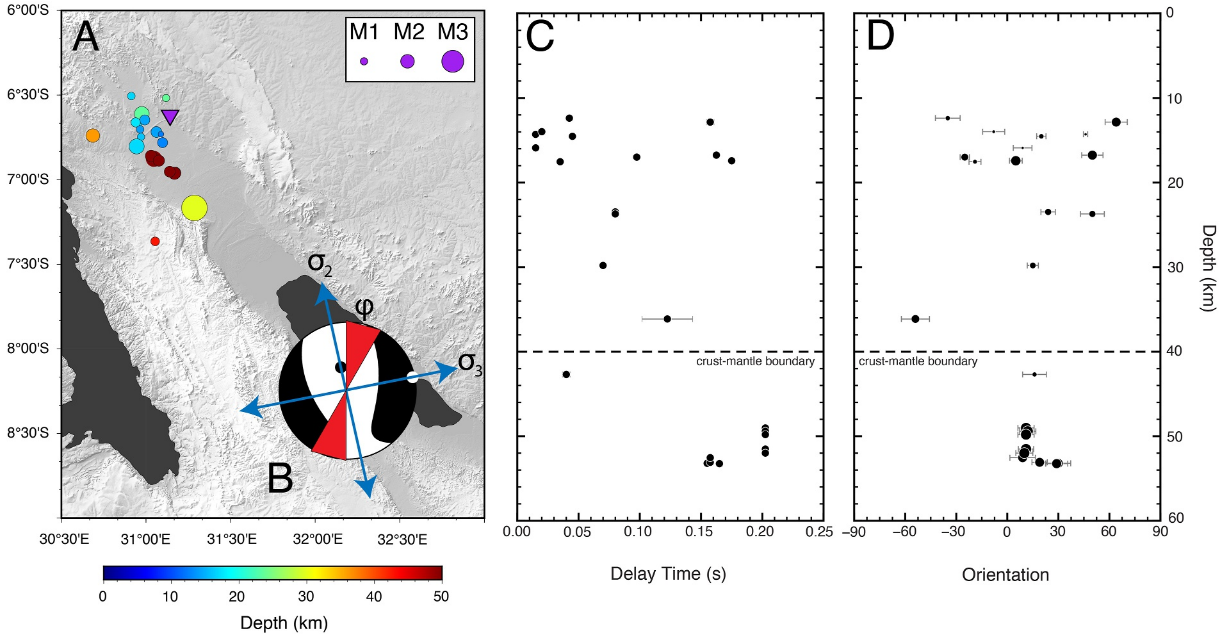

Figure 6. (a) Plot of earthquakes used in the anisotropy study color-coded by depth and scaled by magnitude. (b) Kostrov summation gives P and T axes from teleseisms from 1977 to 2017 that span 8–37 km (Lavayssière et al., 2019). Blue arrows indicate principal stresses from inversion of crustal earthquakes detected on the local array (from Lavayssière et al., 2019). The red area denotes the range of fast direction orientations for upper mantle earthquakes. (c) Delay time (dt) for measurements of seismic anisotropy from earthquakes near station SITA (represented by inverted purple triangle). (d) Variations in azimuth of the fast polarized wave (f). The size of the circle is proportional to the delay time (0.01–0.20 s).

order 1–10 MPa (Figure 7a). For our sill-shaped density contrast, the largest differential stress was ∼2 MPa at the tips of the intrusion (Figures 7f and 7g). The largest stress differential of ∼9.1 MPa is along the edges of a hot dike at 40 km depth and the smallest stress differential of ∼1 MPa is induced by a hot, 2 km by 8 km magmatic complex at 30 km depth where the density contrast is small (∼100 kg/m3). With extensional forces, the differential stresses at the edges of a sill-like intrusion increase to around ∼4 MPa due to the addition of a horizontal stress (Figure 7g). A thinned crust and sill intrusion result in high differential stresses along the edges of the intrusion ∼2 MPa and at the edges of the thinned crust ∼3 MPa. Even a small density contrast (5%) representing a cooled 8 km tall dike in the upper mantle can induce stress concentrations of order ∼3 MPa (Figure 7e). Models with cooled magmatic intrusions in the lower crust have negative (i.e., compressional) stress concentrations due to the intrusions' higher density compared to the surrounding crustal rock. The largest stress differentials in the upper mantle are induced by a magmatic complex or dike of dimensions 8 km by 6 km at 50 km depth with localized stress concentrations of order ∼7 MPa (Figure 7a). As the intrusions cool (i.e., density increases), high differential stresses (>1 MPa) remain concentrated at the edges of the density contrast (Figures 7b–7d)

6.4. Stress Orientations

The reference model assumes lithostatic state-of-stress at every node: vertical stress = horizontal stress in two dimensions. Introducing a density heterogeneity in the model creates zones where vertical stress ≠ horizontal stress due to unbalanced body forces that rotate the principal stress orientation (e.g., Gerya, 2015). Consequently, the degree to which principal stress directions are altered is directly related to the magnitude of the stress differential induced by the density heterogeneity. A greater induced stress differential affects stresses at greater distances. However, it is crucial to recognize that extensional forces are significantly greater in magnitude and thus exert a stronger influence on the regional state of stress (e.g., Oliva et al., 2022).

The principal stress orientations (σ_1) around the density contrasts produce patterns similar to independent measurements of stress patterns around crustal dikes and sills (e.g., Gudmundsson, 2006; Oliva et al., 2022): vertical above, horizontal below, and plunging ∼30° inward along the sides (Figures 8a and 8b). Near the intrusion, the principal stress orientations can be rotated up to 30° in relation to the principal stresses of the reference model (Figures 8a and 8b). Plotting the upper mantle earthquake source mechanisms to depth displays

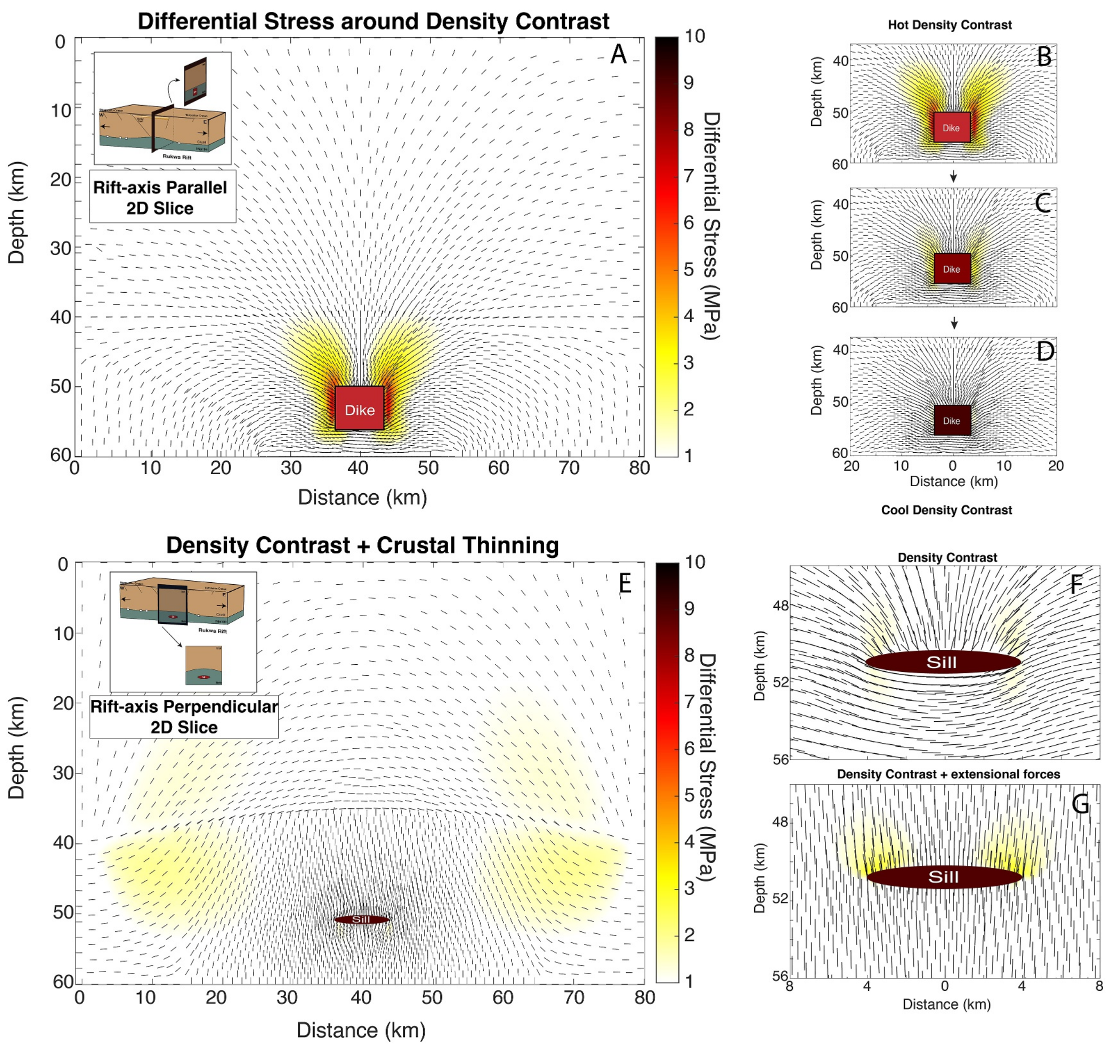

Figure 7. (a) 2D Static numerical model results for an 8 by 6 km magmatic complex or dike placed at 50 km depth with the largest stress differential of ∼7 MPa near the edges of the density contrast. Inset displays the orientation of the 2D model slice in respect to the rift axis. (b)–(d) Represent progressive stages of a cooling magmatic intrusion and the differential stresses and principal stress orientations around the intrusion. (e) 2D Static numerical model results for a sill-shaped intrusion of 2 by 8 km at 50 km depth with a thinned crust. The largest stress differentials ∼2 MPa are near the edges of the density contrast and at the edges of the thinned crust. Inset displays the orientation of the 2D model slice in respect to the rift axis. (f) Differential stresses around a sill-shaped intrusion in the upper mantle and principal stresses around the intrusion. (g) Differential stresses around a sill-shaped intrusion in the upper mantle with extensional forces displaying the principal stresses around the intrusion. Tick marks on all plots represent the orientation of σ_1.

the steep and oblique nodal planes that show similar orientations to the principal stresses around magmatic intrusions (Figures 8a and 8b).

7. Discussion

7.1. Density Contrasts and Upper Mantle Earthquakes

Considering the geochemical evidence for CO_2-rich fluid percolation, seismological evidence for partial melt, evidence for pipelike, upward migrating swarms of mantle earthquakes in the Rwenzori sector of the Western rift (Lindenfeld et al., 2012), and the seismic evidence for a rotated stress field, it is likely that the upper mantle earthquakes are linked to mantle magmatic intrusions that have yet to manifest with surface observations. Although upward migrating swarms of earthquakes are most likely linked to dynamic and active propagating dikes and volatile release, the sporadic, mantle earthquakes in the Tanganyika-Rukwa rift are more likely driven by the presence of static magmatic intrusions that create lateral stress gradients. Based on evidence from ancient rift outcrops these partially molten or frozen magmatic intrusions are lateral density heterogeneities of

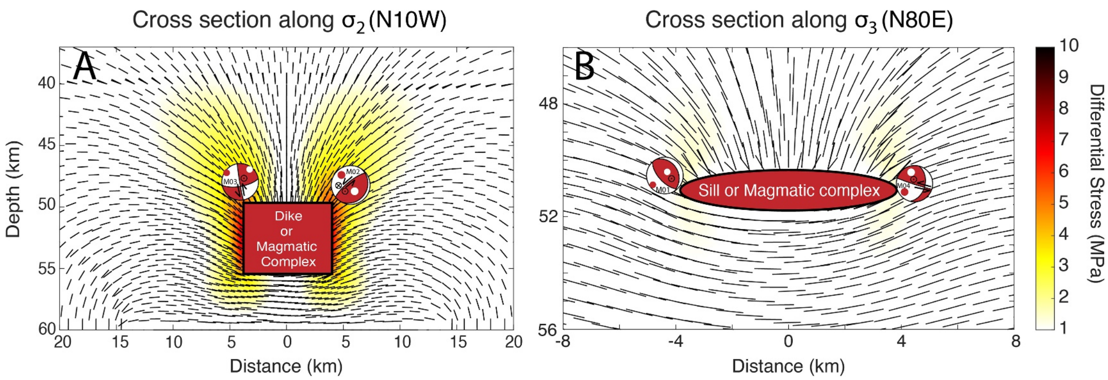

Figure 8. (a) Predictions of principal stress, σ_1, orientations around a hot, 8 km by 6 km dike or sill complex at 50 km depth. The earthquake source mechanisms (M02, M03) around the intrusions are plotted to depth based on the cross section along σ_2 (N10 W) on Figure 5. (b) Predictions of principal stress, σ_1, orientations around a hot, 2 km by 8 km sill-shaped intrusion at 50 km depth. The earthquake source mechanisms (M01, M04) around the intrusions are plotted to depth based on the cross section along σ_3 (N80 E) on Figure 5. Focal mechanisms have ↿|⇂ and/or ⊙/⊗ to show fault plane and slip direction. Plot demonstrates that regions of density contrast induce rotations in local stress orientations and have high stress concentrations near the edges of the intrusion and show that the upper mantle source mechanisms match the principal stress orientations around the intrusions.

considerable spatial extent. The heterogeneous density material is broader than the intruded zone owing to contact metamorphism that produces weaker minerals than the original peridotite (e.g., Sørensen et al., 2019).

Through extensive tests of model geometries, density contrasts, and depth emplacements we identified threshold dimensions of 2 × 8 km required to generate subsurface stress concentrations of at least 1 MPa. This area is consistent with the dimensions of seismically imaged frozen sills in the mantle beneath a mid-ocean ridge (e.g., Qin et al., 2020). These differential stresses are in addition to plate tectonic stresses. Our static models are, therefore, a viable way of explaining mantle earthquakes as induced stresses from subsurface lateral density contrasts. We suggest that the stress concentrations along the margins of density contrasts are then released through seismogenesis, as the modeled stress magnitudes are in the range of earthquake stress drops for small magnitude earthquakes (e.g., Baltay et al., 2024). It is important to note, however, that stress drop remains a poorly constrained variable with significant uncertainties (e.g., Abercrombie et al., 2025). Furthermore, the depth of the upper mantle earthquakes affects these estimates, as stress drop calculations may be further influenced by seismic attenuation and near-source structural effects (Abercrombie et al., 2021).

The body forces from magmatic intrusions cause local rotations in the stress field that are consistent with indicators of mantle state-of-stress: shear-wave splitting and earthquake source mechanisms that show rotations from the regional sub-E–W stress field (Figures 7 and 8). Specifically, if the fast orientation of shear waves was controlled by the orientation of fractures in the lower crust and mantle, we would anticipate that the fast orientation would be oriented in the direction perpendicular to σ_3, the extension direction in the region. Given that σ_3 is oriented N80°E, we would expect a fast orientation of N10°W. However, our study shows that the observed anisotropy in the upper mantle deviates by up to 30° from this expected orientation, suggesting a local rotation of the mantle stress field relative to the regional tectonic stress orientation derived from teleseisms (Figure 6b). Direct comparison with focal mechanism solutions would require mantle imaging of the geometry of the intruded body (ies), which is not available. If we assume that some of the earthquake source mechanisms lie along the edges of the intruded body (ies), we would expect rotated P- and T-axes that align with the local stress field around the intrusion(s). The fault and auxiliary plane of all upper mantle source mechanisms show a poor agreement with the regional tectonic stress derived from teleseisms and with the shear-wave splitting results (Figure SM4 in Supporting Information S1). However, the P- and T-axes from the source mechanisms are consistent with those expected near the principal stress directions around the edges of a magmatic intrusion (Figure 8). It is important to note that the stress field around the density contrast is projected in two dimensions which leaves the third dimension unconstrained. Some focal mechanisms have P- and T-axes that have an out-of-plane component in a cross-sectional view (Figure 8). However, it is clear that there are rotations in the P-axis across the focal mechanisms. For example, event M01 has the P-axis or σ_1 oriented along the regional stress σ_3 (Figure 8). Having only four earthquakes, and none with surface waves adequate for waveform modeling, we can only comment that each source mechanism has one near-vertical nodal plane that can be placed along the margins of the density contrast.

Ancient rift zones provide additional insights. The presence of pseudo-tachylites, formed by shear heating and quenching during earthquakes, along the margins of magma intrusions in upper mantle rocks exposed in Norway's Caledonide orogeny confirm that boundaries of upper mantle intrusions are seismogenic (Sørensen et al., 2019). Petrological analyses of contact aureoles around the mantle intrusions show dolomite replacement of olivine; dolomite is an order of magnitude weaker than olivine and dolomite formation is a volumetric expansion that may cause fracturing and grain size reduction (Sørensen et al., 2019). Additionally, CO_2 reactions lead to brittle fracturing of olivine in mantle rock (Sørensen et al., 2019). CO_2-rich magmas in the Western rift volcanic provinces indicate that the Caledonide sites could be analogous (e.g., Furman, 1995; Innocenzi et al., 2024).

The modeling results indicate that induced stress differentials are comparable to earthquake stress drops, but are the forces adequate to rupture strong mantle? The combination of local mantle strength reduction through metasomatic reactions and body forces from magmatic intrusions (i.e., density contrasts) may be enough to cause earthquakes in uppermost mantle rocks. Additionally, other factors may directly or indirectly augment local stresses such as high pore fluid pressures and far-field extensional forces. Including both of these effects further strengthens the possibility that static density contrasts are responsible for the upper mantle earthquakes in the Tanganyika-Rukwa rift and justifying the comparison to pseudo-tachylites in the Caledonide rift zone.

7.2. Can Upper Mantle Earthquakes Connect to Border Faults and Rupture to the Surface?

The Tanganyika-Rukwa rift has seismogenic activity spanning the near surface to the base of the crust (Figure 2). The most energetic earthquakes occur in the lower crust (Lavayssière et al., 2019; Yang & Chen, 2010), consistent with a strong and relatively cold lower crust and uppermost mantle (e.g., Ebinger et al., 1991). Border faults in the Western rift form very early during rifting and remain the locus of deformation for >10 My of rifting, with >M6 lower crustal earthquakes rupturing large sections of the ~100 km-long border faults. The upper mantle earthquakes we recorded occurred beneath a relatively young normal fault system that kinematically links the Rukwa and Tanganyika rifts (Figure 1b). Although we cannot determine whether magma intrusion beneath the uplifted flank of the southern Tanganyika rift facilitated border fault development, the lower crustal earthquakes and mantle earthquakes occur in close proximity to the border fault, suggesting that the strain concentrations along the margins of active and cooled magmatic intrusions may help localize strain to border faults (Figures 2 and 8), and as discussed below. The M7.4 1910 Rukwa earthquake that triggered a landslide in the Indian Ocean (Ambraseys, 1991) occurred in the same area, and the mantle earthquakes we report provoke the question: Did the 1910 earthquake initiate in the upper mantle? Regardless of causative mechanism, these results inform hazard mitigation in weakly extended rift zones.

7.3. Magmatic Intrusions in Continental Rift Zones

Rifting in thick, strong cold lithosphere in stable continental interiors is a geodynamic enigma: the strength of the cold, thick continental plates is larger than the forces available (e.g., Bialas et al., 2010). However, the mantle lithosphere intrusions, both active or frozen, and metasomatic reactions around the intrusions simulated in this study would lead to mantle strength reductions. These weaker and localized regions near magmatic intrusions then become the locus of strain. In the Tanganyika-Rukwa rift, the upper mantle earthquakes are in close proximity to the border faults (Figure 2). Magmatic systems lead to stress concentrations that guide subsequent intrusions and influence the formation of new faults and fractures as predicted for more highly extended rifts (e.g., Buck, 2004; Gudmundsson, 2006). The addition of heat and volatiles at the base of the crust, near the border faults, may contribute to the stabilization of crustal-scale border faults for time periods >10 My (e.g., Ebinger et al., 1991), rather than migrating to conjugate or new border faults outboard of the older fault, as predicted in numerical models (e.g., Phillips et al., 2023).

Furthermore, our models with crustal thinning and extensional forces show that these additional components can augment differential stresses. As a result, the stress concentrations along the edges of magmatic complexes may be higher than what the model predicts due to the horizontal pulling forces on a plate. Crustal thinning itself is a form of a large density heterogeneity which produces large differential stresses near the border faults as seen on Figure 7e. It is important to note, however, that the magnitude of the calculated differential stress is sensitive to both the geometry of the Moho and the parameterization and discretization of the finite element model. The combinations of lateral density variations, crustal thinning and horizontal forces all contribute to a complex subsurface state-of-stress (e.g., Oliva et al., 2022).

8. Conclusions

We investigate the possibility that upper mantle earthquakes beneath the Tanganyika-Rukwa rift are linked to lower crustal and upper mantle magmatic intrusions that cause pressure gradients that concentrate stress. Evidence for such localized stress field rotations beneath the Tanganyika-Rukwa rift comes from shear wave splitting and source mechanisms from local earthquakes. Using numerical models, we explore whether these earthquakes result from localized stress concentrations caused by density contrasts of considerable spatial extent, augmented by strength reductions in the contact aureole surrounding the intrusions. Our 2D PyLith elastic simulations are based on geologically constrained models of dike and sill complexes. Each simulation produces static stress concentrations between 1 and 10 MPa, with the highest (~9.1 MPa) occurring along the edges of an 8 km by 6 km (dike) density contrast at the crust-mantle boundary depths. Our simulated intrusions with shapes, sizes, and locations representative of geologic dike and sill complexes, generate differential stresses in the range of earthquake stress drops. Moreover, our models indicate that these large differential stresses can induce significant rotations in the local stress field. The rotated, sub-vertical principal stress orientations at the edges of the magmatic bodies may guide the location and upward path of magma intrusion and increase stress near crustal fault systems. These deep, and therefore difficult to detect, magmatic systems may provide a mechanism for upper mantle earthquakes in weakly extended rift zones. The close proximity of mantle earthquakes to crustal-scale border fault systems suggests that intrusions may help localize strain to border faults and increase the risk of M > 7 earthquakes in cratonic rifts.

Conflict of Interest

The authors declare no conflicts of interest relevant to this study.

Availability Statement

Earthquake waveform data analyzed in this study are available at Ebinger, C. J. (2014). The TANGA14 complete catalog is available in the supplementary material of Lavayssière et al. (2019). PyLith scripts are available at Earzabala (2026).

Acknowledgments
We are grateful to Associate Editor Rachel Abercrombie, Will Levandowski, and an anonymous reviewer for thoughtful and constructive feedback that refined and sharpened our arguments. EA and CE were partially supported by the U.S. – Israel Center for Fossil Energy (FEC-19), funded by the U.S. Department of Energy, the Israel Energy Ministry and administered by the BIRD foundation and NSF grant EAR-2039963. EA is partially supported by the Bill and Melinda Gates Foundation as a Gates Millennium Scholar. CE thanks the Marshall-Heape Fund at Tulane University. We thank the Computational Infrastructure for Geodynamics (http://geodynamics.org) which is funded by the National Science Foundation under awards EAR-0949446 and EAR-1550901, and EAR-2149126 for the PyLith software and tutorial workshops (Golden, CO).

References

Aagaard, B., Knepley, M., & Williams, C. (2024). Geodynamics/pylith v4.2.0 [Software]. *Zenodo*. https://doi.org/10.5281/zenodo.14635926

Abercrombie, R. E., Baltay, A., Chu, S., Taira, T., Bindi, D., Boyd, O. S., et al. (2025). Overview of the SCEC/USGS community stress drop validation study using the 2019 ridgecrest earthquake sequence. *Bulletin of the Seismological Society of America*, *115*(3), 734–759. https://doi.org/10.1785/0120240158

Abercrombie, R. E., Trugman, D. T., Shearer, P. M., Chen, X., Zhang, J., Pennington, C. N., et al. (2021). Does earthquake stress drop increase with depth in the crust? *Journal of Geophysical Research: Solid Earth*, *126*(10), e2021JB022314. https://doi.org/10.1029/2021JB022314

Afonso, J. C., Ben-Mansour, W., O'Reilly, S. Y., Griffin, W. L., Salajegheh, F., Foley, S., et al. (2022). Thermochemical structure and evolution of cratonic lithosphere in central and southern Africa. *Nature Geoscience*, *15*(5), 405–410. https://doi.org/10.1038/s41561-022-00929-y

Ajala, R., Kolawole, F., & Menke, W. (2024). Blind magmatism abets nonvolcanic continental rifting. *Communications Earth and Environment*, *5*(1), 1–8. https://doi.org/10.1038/s43247-024-01244-7

Albaric, J., Perrot, J., Déverchère, J., Deschamps, A., Le Gall, B., Ferdinand, R. W., et al. (2010). Contrasted seismogenic and rheological behaviours from shallow and deep earthquake sequences in the North Tanzanian Divergence, East Africa. *Journal of African Earth Sciences*, *58*(5), 799–811. https://doi.org/10.1016/j.jafrearsci.2009.09.005

Ambraseys, N. n. (1991). The Rukwa earthquake of 13 December 1910 in East Africa. *Terra Nova*, *3*(2), 202–211. https://doi.org/10.1111/j.1365-3121.1991.tb00873.x

Baltay, A., Abercrombie, R., Chu, S., & Taira, T. (2024). The SCEC/USGS community stress drop validation Study using the 2019 ridgecrest earthquake sequence. *Seismica*, *3*(1). https://doi.org/10.26443/seismica.v3i1.1009

Belachew, M., Ebinger, C., Coté, D., Keir, D., Rowland, J. V., Hammond, J. O. S., & Ayele, A. (2011). Comparison of dike intrusions in an incipient seafloor-spreading segment in Afar, Ethiopia: Seismicity perspectives. *Journal of Geophysical Research*, *116*(B6), B06405. https://doi.org/10.1029/2010JB007908

Beutel, E., van Wijk, J., Ebinger, C., Keir, D., & Agostini, A. (2010). Formation and stability of magmatic segments in the Main Ethiopian and Afar rifts. *Earth and Planetary Science Letters*, *293*(3), 225–235. https://doi.org/10.1016/j.epsl.2010.02.006

Bialas, R. W., Buck, W. R., & Qin, R. (2010). How much magma is required to rift a continent? *Earth and Planetary Science Letters*, *292*(1), 68–78. https://doi.org/10.1016/j.epsl.2010.01.021

Blanchette, A. R., Klemperer, S. L., Mooney, W. D., & Zahran, H. M. (2018). Two-stage Red Sea rifting inferred from mantle earthquakes in Neoproterozoic lithosphere. *Earth and Planetary Science Letters*, *497*, 92–101. https://doi.org/10.1016/j.epsl.2018.05.048

Boness, N. L., & Zoback, M. D. (2006). Mapping stress and structurally controlled crustal shear velocity anisotropy in California. *Geology*, *34*(10), 825–828. https://doi.org/10.1130/G22309.1

Boniface, N., Schenk, V., & Appel, P. (2014). Mesoproterozoic high-grade metamorphism in pelitic rocks of the northwestern Ubendian Belt: Implication for the extension of the Kibaran intra-continental basins to Tanzania. *Precambrian Research*, *249*, 215–228. https://doi.org/10.1016/j.precamres.2014.05.010

Bott, M. H. P. (1990). Stress distribution and plate boundary force associated with collision mountain ranges. *Tectonophysics*, *182*(3–4), 193–209. https://doi.org/10.1016/0040-1951(90)90163-3

Boyce, A., Kounoudis, R., Bastow, I. D., Cottaar, S., Ebinger, C. J., & Ogden, C. S. (2023). Mantle wavespeed and discontinuity structure below East Africa: Implications for Cenozoic hotspot tectonism and the development of the Turkana depression. *Geochemistry, Geophysics, Geosystems*, *24*(8), e2022GC010775. https://doi.org/10.1029/2022GC010775

Brocher, T. M. (2005). Empirical relations between elastic wavespeeds and density in the Earth's crust. *Bulletin of the Seismological Society of America*, *95*(6), 2081–2092. https://doi.org/10.1785/0120050077

Brown, L. D., & Kim, D. (2020). Extensive sills in the continental basement from deep seismic reflection profiling. *Geosciences*, *10*(11), 449. https://doi.org/10.3390/geosciences10110449

Buck, W. R. (2004). 1. Consequences of asthenospheric variability on Continental rifting. In *1. Consequences of asthenospheric variability on Continental rifting* (pp. 1–30). Columbia University Press. https://doi.org/10.7312/karn12738-002

Bürgmann, R., & Dresen, G. (2008). Rheology of the lower crust and upper mantle: Evidence from rock mechanics, geodesy, and field observations. *Annual Review of Earth and Planetary Sciences*, *36*(1), 531–567. https://doi.org/10.1146/annurev.earth.36.031207.124326

Chang, S.-J., Kendall, E., Davaille, A., & Ferreira, A. M. G. (2020). The evolution of mantle plumes in East Africa. *Journal of Geophysical Research: Solid Earth*, *125*(12), e2020JB019929. https://doi.org/10.1029/2020JB019929

Craig, T. J., & Jackson, J. A. (2021). Variations in the seismogenic thickness of East Africa. *Journal of Geophysical Research: Solid Earth*, *126*(3), e2020JB020754. https://doi.org/10.1029/2020JB020754

Crampin, S., & Peacock, S. (2008). A review of the current understanding of seismic shear-wave splitting in the Earth's crust and common fallacies in interpretation. *Wave Motion*, *45*(6), 675–722. https://doi.org/10.1016/j.wavemoti.2008.01.003

Delvaux, D., Kervyn, F., Macheyeki, A. S., & Temu, E. B. (2012). Geodynamic significance of the TRM segment in the East African Rift (W-Tanzania): Active tectonics and paleostress in the Ufipa plateau and Rukwa basin. *Journal of Structural Geology*, *37*, 161–180. https://doi.org/10.1016/j.jsg.2012.01.008

Déverchère, J., Houdry, F., Diament, M., Solonenko, N. V., & Solonenko, A. V. (1991). Evidence for a seismogenic upper mantle and lower crust in the Baikal Rift. *Geophysical Research Letters*, *18*(6), 1099–1102. https://doi.org/10.1029/91GL00851

Dunn, R. A., Lekić, V., Detrick, R. S., & Toomey, D. R. (2005). Three-dimensional seismic structure of the Mid-Atlantic Ridge (35°N): Evidence for focused melt supply and lower crustal dike injection. *Journal of Geophysical Research*, *110*(B9), B09101. https://doi.org/10.1029/2004JB003473

Earzabala. (2026). earzabala/Testing-Models-for-Upper-Mantle-Earthquakes-in-the-Tanganyika-Rukwa-Rift-Africa: PyLith Scripts (1.0) [Software]. *Zenodo*. https://doi.org/10.5281/zenodo.18777610

Ebinger, C. J. (2014). Southern Lake Tanganyika experiment [Dataset]. *International Federation of Digital Seismograph Networks*. https://doi.org/10.7914/SN/ZV_2014

Ebinger, C. J., Karner, G. D., & Weissel, J. K. (1991). Mechanical strength of extended continental lithosphere: Constraints from the Western Rift System, East Africa. *Tectonics*, *10*(6), 1239–1256. https://doi.org/10.1029/91TC00579

Ebmeier, S. K., Andrews, B. J., Araya, M. C., Arnold, D. W. D., Biggs, J., Cooper, C., et al. (2018). Synthesis of global satellite observations of magmatic and volcanic deformation: Implications for volcano monitoring and the lateral extent of magmatic domains. *Journal of Applied Volcanology*, *7*(1), 2. https://doi.org/10.1186/s13617-018-0071-3

Fialko, Y. A., & Rubin, A. M. (1999). Thermal and mechanical aspects of magma emplacement in giant dike swarms. *Journal of Geophysical Research*, *104*(B10), 23033–23049. https://doi.org/10.1029/1999JB900213

Furman, T. (1995). Melting of metasomatized subcontinental lithosphere: Undersaturated mafic lavas from Rungwe, Tanzania. *Contributions to Mineralogy and Petrology*, *122*(1), 97–115. https://doi.org/10.1007/s004100050115

Gaherty, J., Ebinger, C., Nyblade, A., & Shillington, D. (2013). Study of extension and maGmatism in Malawi aNd Tanzania [Dataset]. *International Federation of Digital Seismograph Networks*. https://doi.org/10.7914/SN/YQ_2013

Gase, A. C., Van Avendonk, H. J., Bangs, N. L., Luckie, T. W., Barker, D. H., Henrys, S. A., et al. (2019). Seismic evidence of magmatic rifting in the offshore Taupo Volcanic Zone, New Zealand. *Geophysical Research Letters*, *46*(22), 12949–12957. https://doi.org/10.1029/2019gl085269

Gerya, T. (2015). Tectonic overpressure and underpressure in lithospheric tectonics and metamorphism. *Journal of Metamorphic Geology*, *33*(8), 785–800. https://doi.org/10.1111/jmg.12144

Geuzaine, C., & Remacle, J.-F. (2009). Gmsh: A 3-D finite element mesh generator with Built-in Pre- and post-processing facilities. *International Journal for Numerical Methods in Engineering*, *79*(11), 1309–1331. https://doi.org/10.1002/nme.2579

Gudmundsson, A. (2006). How local stresses control magma-chamber ruptures, dyke injections, and eruptions in composite volcanoes. *Earth-Science Reviews*, *79*(1), 1–31. https://doi.org/10.1016/j.earscirev.2006.06.006

Hodgson, I., Illsley-Kemp, F., Gallacher, R., Keir, D., Ebinger, C., & Mtelela, K. (2017). Crustal structure at a young Continental rift: A receiver function Study from the Tanganyika rift: Crustal structure at the Tanganyika rift. *Tectonics*, *36*(12), 2806–2822. https://doi.org/10.1002/2017TC004477

Hutchings, S. J., Koper, K. D., Burlacu, R., Zeng, Q., Lin, F. C., & Zandt, G. (2025). Upper mantle earthquakes along the edge of the Wyoming Craton. *Geophysical Research Letters*, *52*(9), e2024GL114073. https://doi.org/10.1029/2024gl114073

Illsley-Kemp, F., Savage, M. K., Wilson, C. J. N., & Bannister, S. (2019). Mapping stress and structure from subducting slab to magmatic rift: Crustal seismic anisotropy of the North Island, New Zealand. *Geochemistry, Geophysics, Geosystems*, *20*(11), 5038–5056. https://doi.org/10.1029/2019GC008529

Illsley-Kemp, F., Savage, M. K., Keir, D., Hirschberg, H. P., Bull, J. M., Gernon, T. M., et al. (2017). Extension and stress during continental breakup: Seismic anisotropy of the crust in Northern Afar. *Earth and Planetary Science Letters*, *477*, 41–51. https://doi.org/10.1016/j.epsl.2017.08.014

Innocenzi, F., Ronca, S., Foley, S., Agostini, S., & Lustrino, M. (2024). Carbonatite and ultrabasic magmatism at Toro Ankole and Virunga, western branch of the East African Rift system. *Gondwana Research*, *125*, 317–342. https://doi.org/10.1016/j.gr.2023.09.005

Jolly, R. J. H., & Sanderson, D. J. (1995). Variation in the form and distribution of dykes in the Mull swarm, Scotland. *Journal of Structural Geology*, *17*(11), 1543–1557. https://doi.org/10.1016/0191-8141(95)00046-G

Kendall, J.-M., Pilidou, S., Keir, D., Bastow, I. D., Stuart, G. W., & Ayele, A. (2006). Mantle upwellings, melt migration and the rifting of Africa: Insights from seismic anisotropy. *Geological Society, London, Special Publications*, *259*(1), 55–72. https://doi.org/10.1144/GSL.SP.2006.259.01.06

Lavayssière, A., Drooff, C., Ebinger, C., Gallacher, R., Illsley-Kemp, F., Oliva, S. J., & Keir, D. (2019). Depth extent and kinematics of faulting in the Southern Tanganyika rift, Africa. *Tectonics*, *38*(3), 842–862. https://doi.org/10.1029/2018TC005379

Lindenfeld, M., Rümpker, G., Link, K., Koehn, D., & Batte, A. (2012). Fluid-triggered earthquake swarms in the Rwenzori region, East African Rift—Evidence for rift initiation. *Tectonophysics*, *566–567*, 95–104. https://doi.org/10.1016/j.tecto.2012.07.010

Magee, C., Hunt-Stewart, E., & Jackson, C. A.-L. (2013). Volcano growth mechanisms and the role of sub-volcanic intrusions: Insights from 2D seismic reflection data. *Earth and Planetary Science Letters*, *373*, 41–53. https://doi.org/10.1016/j.epsl.2013.04.041

Magee, C., Muirhead, J. D., Karvelas, A., Holford, S. P., Jackson, C. A., Bastow, I. D., et al. (2016). Lateral magma flow in mafic sill complexes. *Geosphere*, *12*(3), 809–841. https://doi.org/10.1130/ges01256.1

Menegon, L., Campbell, L., Mancktelow, N., Camacho, A., Wex, S., Papa, S., et al. (2021). The earthquake cycle in the dry lower continental crust: Insights from two deeply exhumed terranes (Musgrave Ranges, Australia and Lofoten, Norway). *Philosophical Transactions of the Royal Society A: Mathematical, Physical and Engineering Sciences*, *379*(2193), 20190416. https://doi.org/10.1098/rsta.2019.0416

Morley, C. K. (1988). Variable extension in Lake Tanganyika. *Tectonics*, *7*(4), 785–801. https://doi.org/10.1029/TC007i004p00785

Mtelela, C., Roberts, E. M., Downie, R., & Hendrix, M. S. (2016). Interplay of structural, climatic, and volcanic controls on late Quaternary lacustrine–deltaic sedimentation patterns in the Western branch of the East African rift System, Rukwa rift Basin, Tanzania. *Journal of Sedimentary Research*, *86*(10), 1179–1207. https://doi.org/10.2110/jsr.2016.73

Muirhead, J. D., Wright, L. J. M., & Scholz, C. A. (2019). Rift evolution in regions of low magma input in East Africa. *Earth and Planetary Science Letters*, *506*, 332–346. https://doi.org/10.1016/j.epsl.2018.11.004

Oliva, S. J., Ebinger, C. J., Rivalta, E., Williams, C. A., Wauthier, C., & Currie, C. A. (2022). State of stress and stress rotations: Quantifying the role of surface topography and subsurface density contrasts in magmatic rift zones (Eastern Rift, Africa). *Earth and Planetary Science Letters*, *584*, 117478. https://doi.org/10.1016/j.epsl.2022.117478

Phillips, T. B., Naliboff, J. B., McCaffrey, K. J., Pan, S., van Hunen, J., & Froemchen, M. (2023). The influence of crustal strength on rift geometry and development–insights from 3D numerical modelling. *Solid Earth*, *14*(4), 369–388. https://doi.org/10.5194/se-14-369-2023

Qin, Y., Singh, S. C., Grevemeyer, I., Marjanović, M., & Roger Buck, W. (2020). Discovery of flat seismic reflections in the mantle beneath the young Juan de Fuca Plate. *Nature Communications*, *11*(1), 1. https://doi.org/10.1038/s41467-020-17946-3

Rivalta, E., Taisne, B., Bunger, A. P., & Katz, R. F. (2015). A review of mechanical models of dike propagation: Schools of thought, results and future directions. *Tectonophysics*, *638*, 1–42. https://doi.org/10.1016/j.tecto.2014.10.003

Roberts, E. M., O'Connor, P. M., Stevens, N. J., Gottfried, M. D., Jinnah, Z. A., Ngasala, S., et al. (2010). Sedimentology and depositional environments of the Red Sandstone Group, Rukwa Rift Basin, southwestern Tanzania: New insight into Cretaceous and Paleogene terrestrial ecosystems and tectonics in sub-equatorial Africa. *Journal of African Earth Sciences*, *57*(3), 179–212. https://doi.org/10.1016/j.jafrearsci.2009.09.002

Roecker, S., Ebinger, C., Tiberi, C., Mulibo, G., Ferdinand-Wambura, R., Mtelela, K., et al. (2017). Subsurface images of the Eastern Rift, Africa, from the joint inversion of body waves, surface waves and gravity: Investigating the role of fluids in early-stage continental rifting. *Geophysical Journal International*, *210*(2), 931–950. https://doi.org/10.1093/gji/ggx220

Rubin, A. M. (1995). Propagation of magma-filled cracks. *Annual Review of Earth and Planetary Sciences*, *23*(1), 287–336. https://doi.org/10.1146/annurev.ea.23.050195.001443

Savage, M. K., Wessel, A., Teanby, N. A., & Hurst, A. W. (2010). Automatic measurement of shear wave splitting and applications to time varying anisotropy at Mount Ruapehu volcano, New Zealand. *Journal of Geophysical Research*, *115*(B12), B12321. https://doi.org/10.1029/2010JB007722

Scholz, C. A., & Lyons, R. P. (2010). New Age estimates for the Lake Malawi rift, East Africa, using deep scientific drill cores and seismic reflection data. *AGU Fall Meeting Abstracts*, T32C-02.

Shillington, D. J., Gaherty, J. B., Ebinger, C. J., Scholz, C. A., Selway, K., Nyblade, A. A., et al. (2016). Acquisition of a unique Onshore/Offshore geophysical and geochemical dataset in the Northern Malawi (Nyasa) rift. *Seismological Research Letters*, *87*(6), 1406–1416. https://doi.org/10.1785/0220160112

Silver, P. G., & Chan, W. W. (1991). Shear wave splitting and subcontinental mantle deformation. *Journal of Geophysical Research*, *96*(B10), 16429–16454. https://doi.org/10.1029/91JB00899

Snoke, J. A. (1984). A program for focal mechanism determination by combined use of polarity and SV-P amplitude ratio data. *Earthquake Notes*, *55*, 15.

Sørensen, B. E., Grant, T., Ryan, E. J., & Larsen, R. B. (2019). In situ evidence of earthquakes near the crust mantle boundary initiated by mantle CO2 fluxing and reaction-driven strain softening. *Earth and Planetary Science Letters*, *524*, 115713. https://doi.org/10.1016/j.epsl.2019.115713

Stamps, D. S., Saria, E., & Kreemer, C. (2018). A geodetic strain rate model for the East African rift System. *Scientific Reports*, *8*(1), 732. https://doi.org/10.1038/s41598-017-19097-w

Teanby, N. A., Kendall, J.-M., & van der Baan, M. (2004). Automation of shear-wave splitting measurements using cluster analysis. *Bulletin of the Seismological Society of America*, *94*(2), 453–463. https://doi.org/10.1785/0120030123

Tepp, G., Ebinger, C. J., Zal, H., Gallacher, R., Accardo, N., Shillington, D. J., et al. (2018). Seismic anisotropy of the upper mantle below the Western rift, East Africa. *Journal of Geophysical Research: Solid Earth*, *123*(7), 5644–5660. https://doi.org/10.1029/2017JB015409

Toda, S., Stein, R. S., & Sagiya, T. (2002). Evidence from the AD 2000 Izu islands earthquake swarm that stressing rate governs seismicity. *Nature*, *419*(6902), 58–61. https://doi.org/10.1038/nature00997

Turcotte, D. L., & Schubert, G. (2002). *Geodynamics* (2nd ed.). Cambridge University Press. https://doi.org/10.1017/CBO9780511807442

Valentine, G. A., & Krogh, K. E. C. (2006). Emplacement of shallow dikes and sills beneath a small basaltic volcanic center – The role of pre-existing structure (Paiute Ridge, southern Nevada, USA). *Earth and Planetary Science Letters*, *246*(3), 217–230. https://doi.org/10.1016/j.epsl.2006.04.031

Wang, S., & Klemperer, S. L. (2026). Continental mantle earthquakes of the world. *Science*, *391*(6785), 611–615. https://doi.org/10.1126/science.adz4367

Weinstein, A., Oliva, S. J., Ebinger, C. J., Roecker, S., Tiberi, C., Aman, M., et al. (2017). Fault-magma interactions during early continental rifting: Seismicity of the magadi-natron-manyara basins, Africa. *Geochemistry, Geophysics, Geosystems*, *18*(10), 3662–3686. https://doi.org/10.1002/2017GC007027

Whitney, D. L., Teyssier, C., Fayon, A. K., Hamilton, M. A., & Heizler, M. (2003). Tectonic controls on metamorphism, partial melting, and intrusion: Timing and duration of regional metamorphism and magmatism in the Niğde Massif, Turkey. *Tectonophysics*, *376*(1), 37–60. https://doi.org/10.1016/j.tecto.2003.08.009

Woods, J., Winder, T., White, R. S., & Brandsdóttir, B. (2019). Evolution of a lateral dike intrusion revealed by relatively-relocated dike-induced earthquakes: The 2014–15 Bárðarbunga–Holuhraun rifting event, Iceland. *Earth and Planetary Science Letters*, *506*, 53–63. https://doi.org/10.1016/j.epsl.2018.10.032

10.1029/2025JB033104

Wrona, T., Magee, C., Fossen, H., Gawthorpe, R. L., Bell, R. E., Jackson, C. L., & Faleide, J. I. (2019). 3-D seismic images of an extensive igneous sill in the lower crust. *Geology*, *47*(8), 729–733. https://doi.org/10.1130/g46150.1

Yang, Z., & Chen, W.-P. (2010). Earthquakes along the East African Rift System: A multiscale, system-wide perspective. *Journal of Geophysical Research*, *115*(B12), B12309. https://doi.org/10.1029/2009JB006779

Zoback, M. L. (1992). First-and second-order patterns of stress in the lithosphere: The World Stress Map Project. *Journal of Geophysical Research*, *97*(B8), 11703–11728. https://doi.org/10.1029/92jb00132